Supplementary Materials for:

"Effect of pH and Molecular Length on Structure and Dynamics of Short Poly(acrylic acid) in Dilute Solution: Detailed Molecular Dynamics Study"

Dimitris G. Mintis[†] and Vlasis G. Mavrantzas[†,§]

[†]Department of Chemical Engineering, University of Patras & FORTH-ICE/HT, Patras, GR26504, Greece

[§]Particle Technology Laboratory, Department of Mechanical and Process Engineering, ETH Zürich, CH-8092 Zürich, Switzerland

S1 Details about Coulomb parameters at different ionization states

S1.1 Completely ionized PAA ($\alpha^{-} = 100\%$)

Coulomb partial charges q (e) on the atoms of a completely ionized PAA chain as computed using different charge techniques are shown in figures S1-S5.

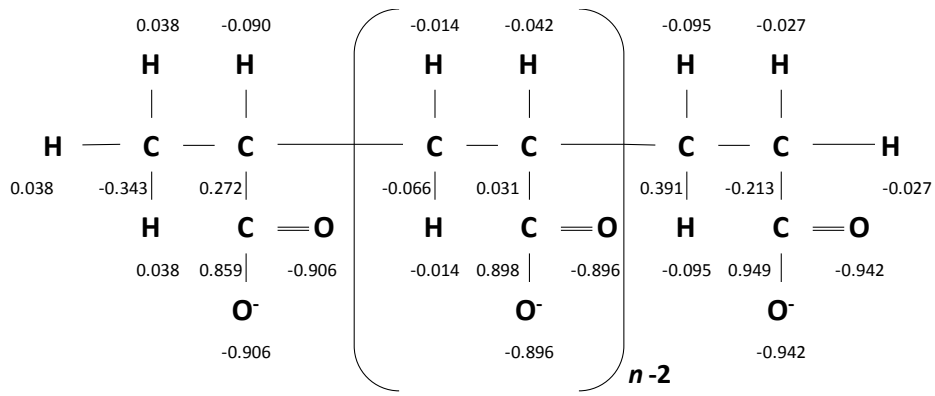

Figure S1: Partial charges based on the RESP charge method.

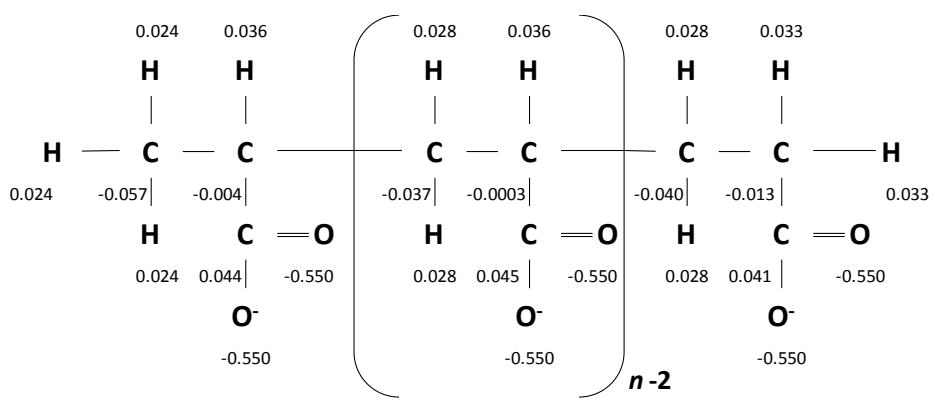

Figure S2: Partial charges based on the Gasteiger charge method.

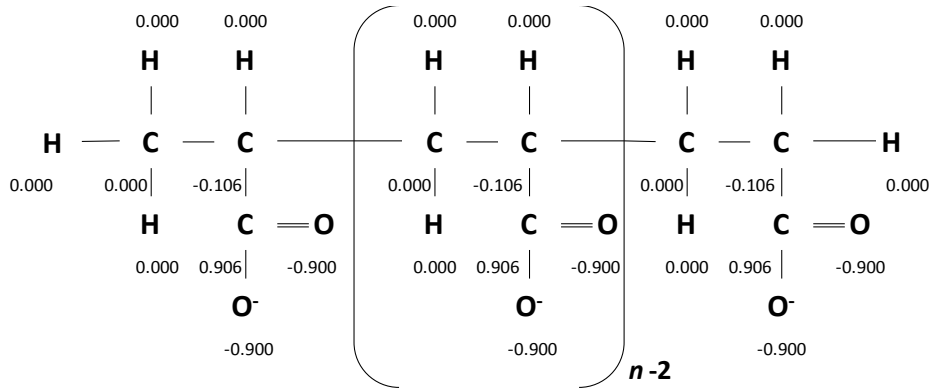

Figure S3: Partial charges based on the bond-increment (BCI) charge method.

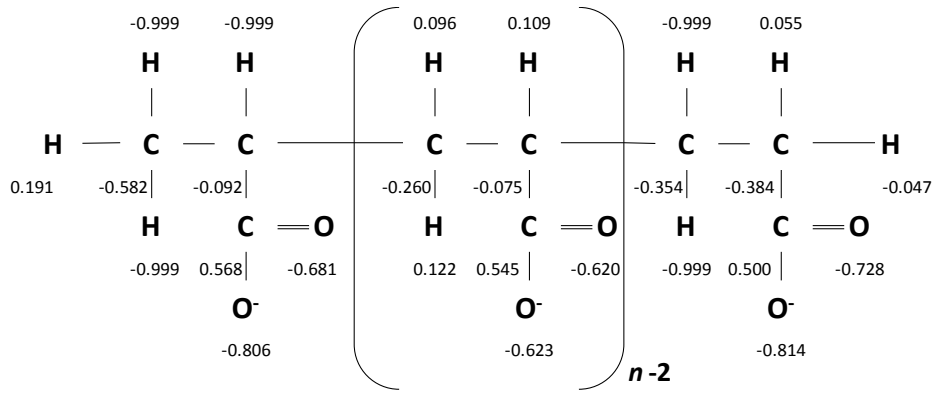

Figure S4: Partial charges based on the QEq charge method.

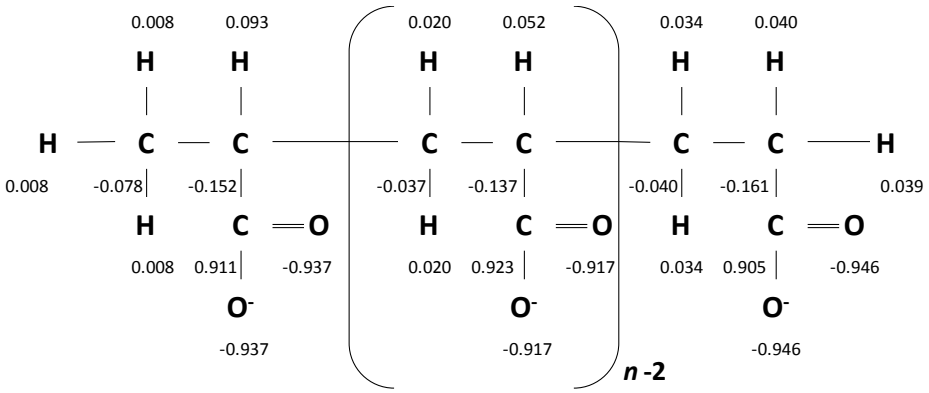

Figure S5: Partial charges based on the AM1-BCC charge method.

S1.2 Alternately ionized PAA ($\alpha^{-} = 50\%$)

Coulomb partial charges q (e) on the atoms of a alternately ionized PAA chain as computed from the RESP fitting method are shown in figure S6.

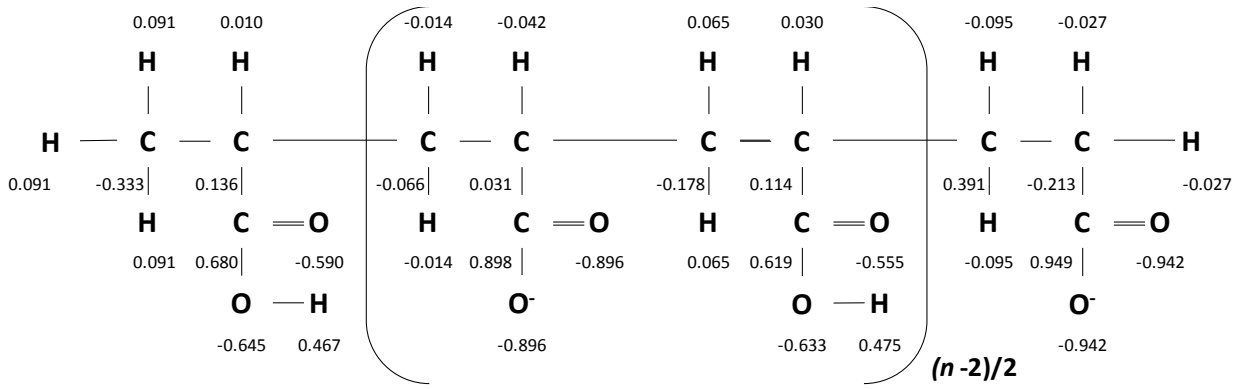

Figure S6: Partial charges based on the RESP charge method.

S1.3 Un-ionized PAA ($\alpha^{-} = 0\%$)

Coulomb partial charges q (e) on the atoms of an un-ionized PAA chain as computed from the RESP fitting method are shown in figure S7.

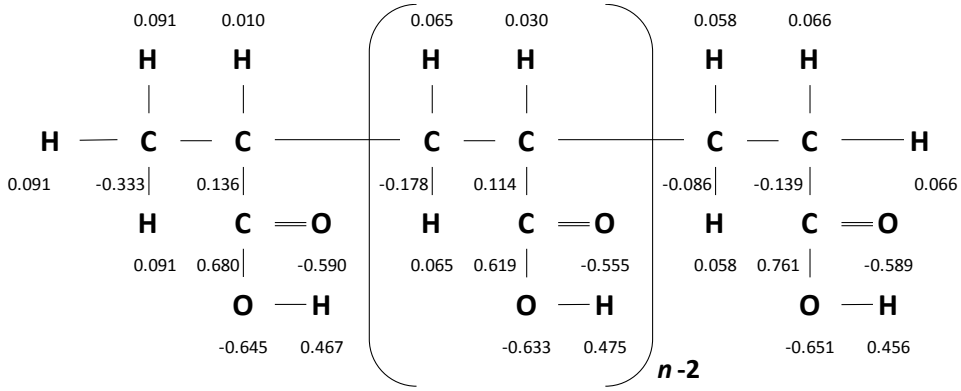

Figure S7: Partial charges based on the RESP charge method.

S2 Lennard-Jones and bonded parameters

In the following figures, we show the atom types at each ionization state.

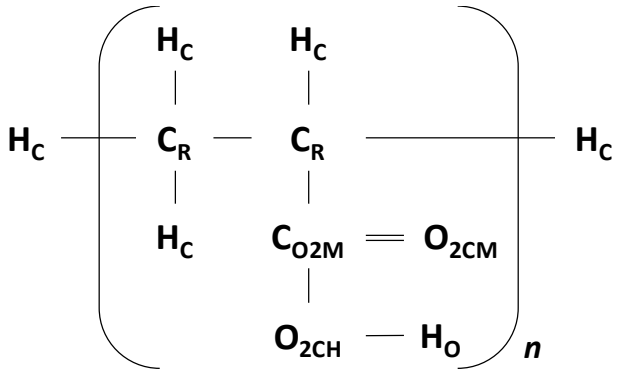

Figure S8: Atom types in a completely ionized PAA chain.

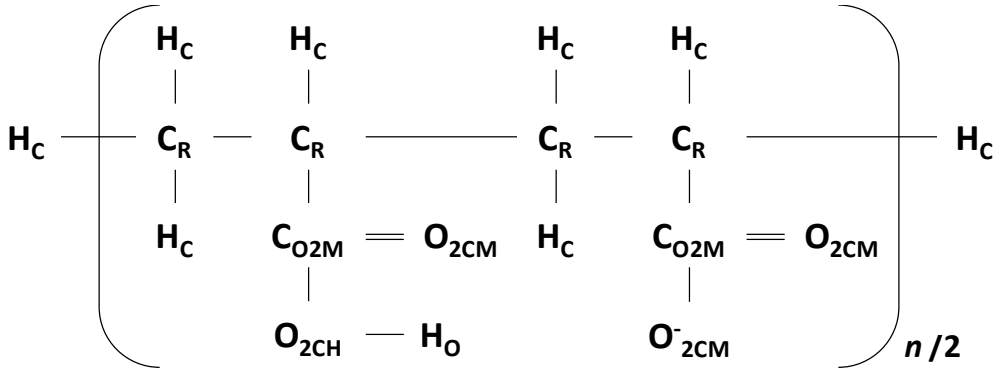

Figure S9: Atom types in an alternately ionized PAA chain.

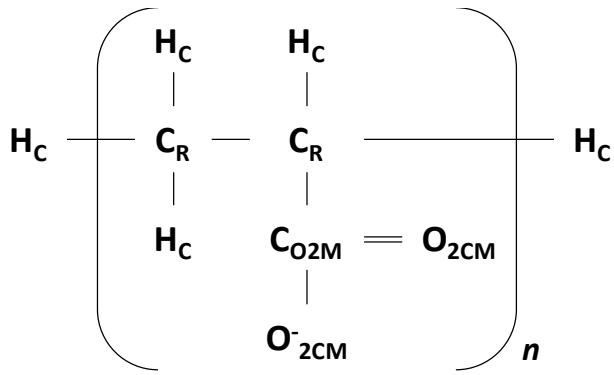

Figure S10: Atom types in an un-ionized (neutral) PAA chain.

Tables S1-S4 show the Lennard-Jones and bonded potential parameters based on the GAFF force field.

Table S1: Lennard-Jones parameters (σ and ε, see eq 3 in the main text) for the atom types shown in figure S10.

Atom type	$\sigma\left(\text{nm}\right)$	$\varepsilon\left(\text{kJ mol}^{-1}\right)$
H_C	0.264953	0.0656888
C_R	0.339967	0.457730
C_{O2M}	0.339967	0.359824
O_{2CM}	0.295992	0.878640
O_{2CH}	0.306647	0.880314
H_O	0.000000	0.000000

Table S2: Bond stretching parameters (b_0 and k_{ij}^{bonds}, see eq 2 in the main text) for bonds between atom types (*ij*) shown in figure S10.

Bond (Atom types, *ij*)	$b_0\left(\text{nm}\right)$	$k_{ij}^{\text{bonds}}\left(\text{kJ mol}^{-1}\text{ nm}^{-2}\right)$
H_C-C_R	0.10920	282250.0
C_R-C_R	0.15350	253630.0
C_R-C_{O2M}	0.13060	390280.0
C_{O2M}-O_{2CM}	0.15080	274720.0
C_{O2M}-O_{2CH}	0.12140	542250.0
O_{2CH}-H_O	0.09740	309280.0

Table S3: Bond angle bending parameters (θ_0 and k_{ijk}^{angle}, see eq 2 in the main text) for angles formed by atom types (*ijk)* shown in figure S10.

Angles (Atom types, *ijk*)	$\theta_0\left(^{\circ}\right)$	$k_{ijk}^{\text{angle}}\left(\text{kJ mol}^{-1}\text{ rad}^{-2}\right)$
H_C-C_R-H_C	108.35	329.95
H_C-C_R-C_R	110.05	388.02
C_R-C_R-C_{O2M}	110.53	533.79
C_R-C_R-C_R	110.63	528.94
H_C-C_R-C_{O2M}	109.68	394.97
C_R-C_{RO2M}-O_{2CM}	123.11	569.28
C_R-C_{O2M}-O_{2CH}	112.20	584.42

O_{2CM}-C_{O2M}-O_{2CM}	130.38	654.13
C_{O2M}-O_{2CH}-H_{O}	107.37	428.36
O_{2CM}-C_{O2M}-O_{2CH}	122.88	647.52

Table S4: Torsional parameters (ϕ_s and $k_{ijkl}^{\text{dihedral}}$, see eq 2 in the main text) for the harmonic potential and the values of the coefficients C_n of the Ryckaert-Bellemans function corresponding to the dihedral angle formed between atom types (*ijkl*) shown in figure S10.

Dihedrals (Atom types, *ijkl*)	$\phi_s\left(\text{deg}\right)$	$k_{ijkl}^{\text{dihedral}}\left(\text{kJ mol}^{-1}\right)$	n
C_R-O_{2CM}-C_{O2M}-O_{2CH}	180.00	4.6024	2

Dihedrals (Atom types, *ijkl*)	$C_0\left(\text{kJ mol}^{-1}\right)$	$C_1\left(\text{kJ mol}^{-1}\right)$	$C_2\left(\text{kJ mol}^{-1}\right)$	$C_3\left(\text{kJ mol}^{-1}\right)$	$C_4\left(\text{kJ mol}^{-1}\right)$	$C_5\left(\text{kJ mol}^{-1}\right)$
H_C-C_R-C_R-H_C	0.62760	1.88280	0.00000	-2.51040	0.00000	0.00000
H_C-C_R-C_R-C_{O2M}	0.65084	1.95253	0.00000	-2.60338	0.00000	0.00000
H_C-C_R-C_R-C_R	0.66944	2.00832	0.00000	-2.67776	0.00000	0.00000
C_R-C_R-C_{O2M}-O_{2CM}	0.00000	0.00000	0.00000	0.00000	0.00000	0.00000
C_R-C_R-C_R-C_R	3.68192	3.09616	-2.09200	-3.01248	0.00000	0.00000
C_R-C_{O2M}-O_{2CH}-H_O	19.2464	0.00000	-19.2464	0.00000	0.00000	0.00000
O_{2CM}-C_{O2M}-O_{2CH}-H_O	27.19600	-7.94960	-19.2464	0.00000	0.00000	0.00000
H_C-C_R-C_{O2M}-O_{2CM}	3.68192	-4.35136	0.00000	1.33888	0.00000	0.00000

S3 Molecular Mechanics Force Field Validation

S3.1 $\left\langle R_{\mathrm{g}}^{2}\right\rangle^{0.5}$ and $\left\langle R_{\mathrm{ee}}^{2}\right\rangle^{0.5}$

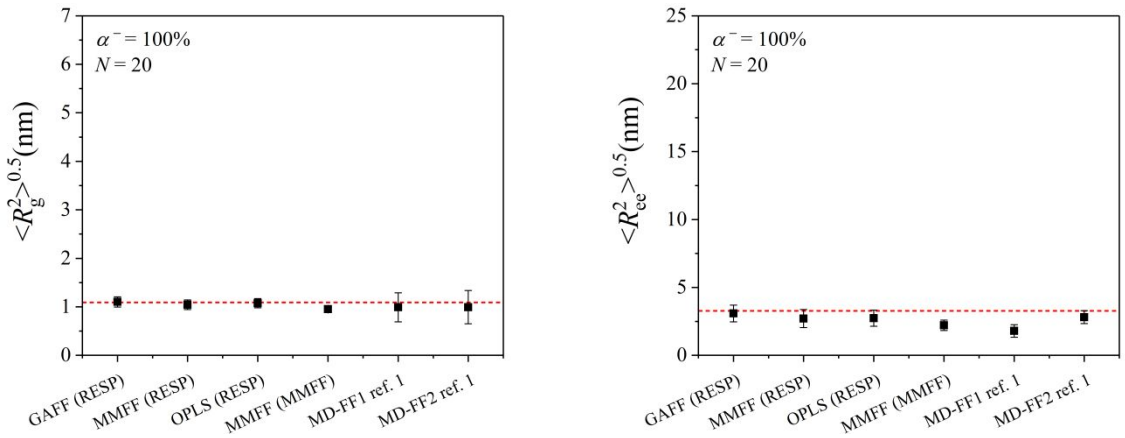

Figure S 11. Comparison of the MD predictions for $\left\langle R_{\mathrm{g}}^{2}\right\rangle^{0.5}$ and $\left\langle R_{\mathrm{ee}}^{2}\right\rangle^{0.5}$ against reference value[1] for several molecular mechanics force fields in combination with various charge techniques and water models.

S3.2 Intermolecular radial distribution functions

S3.2.1 Cb-Ow

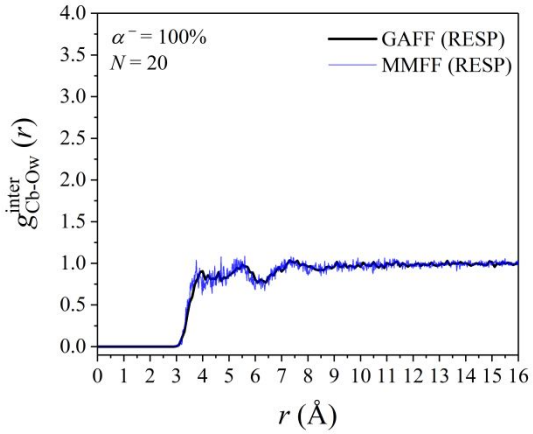

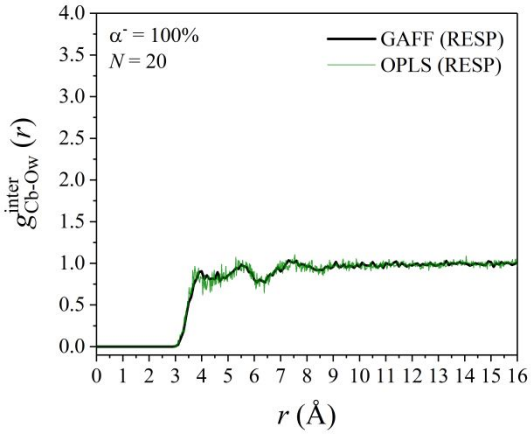

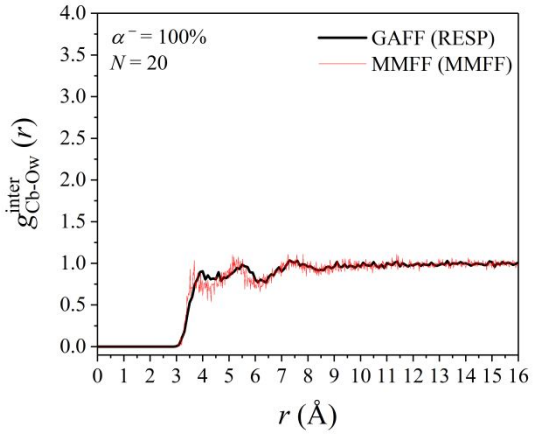

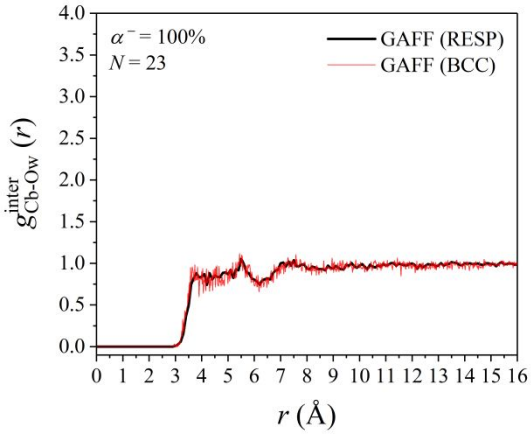

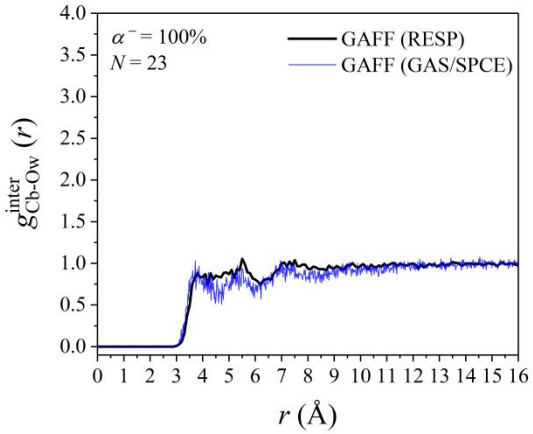

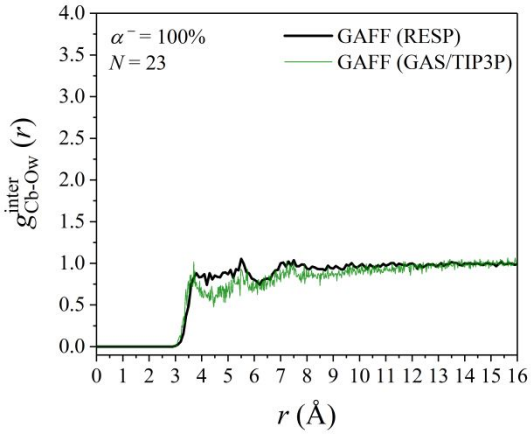

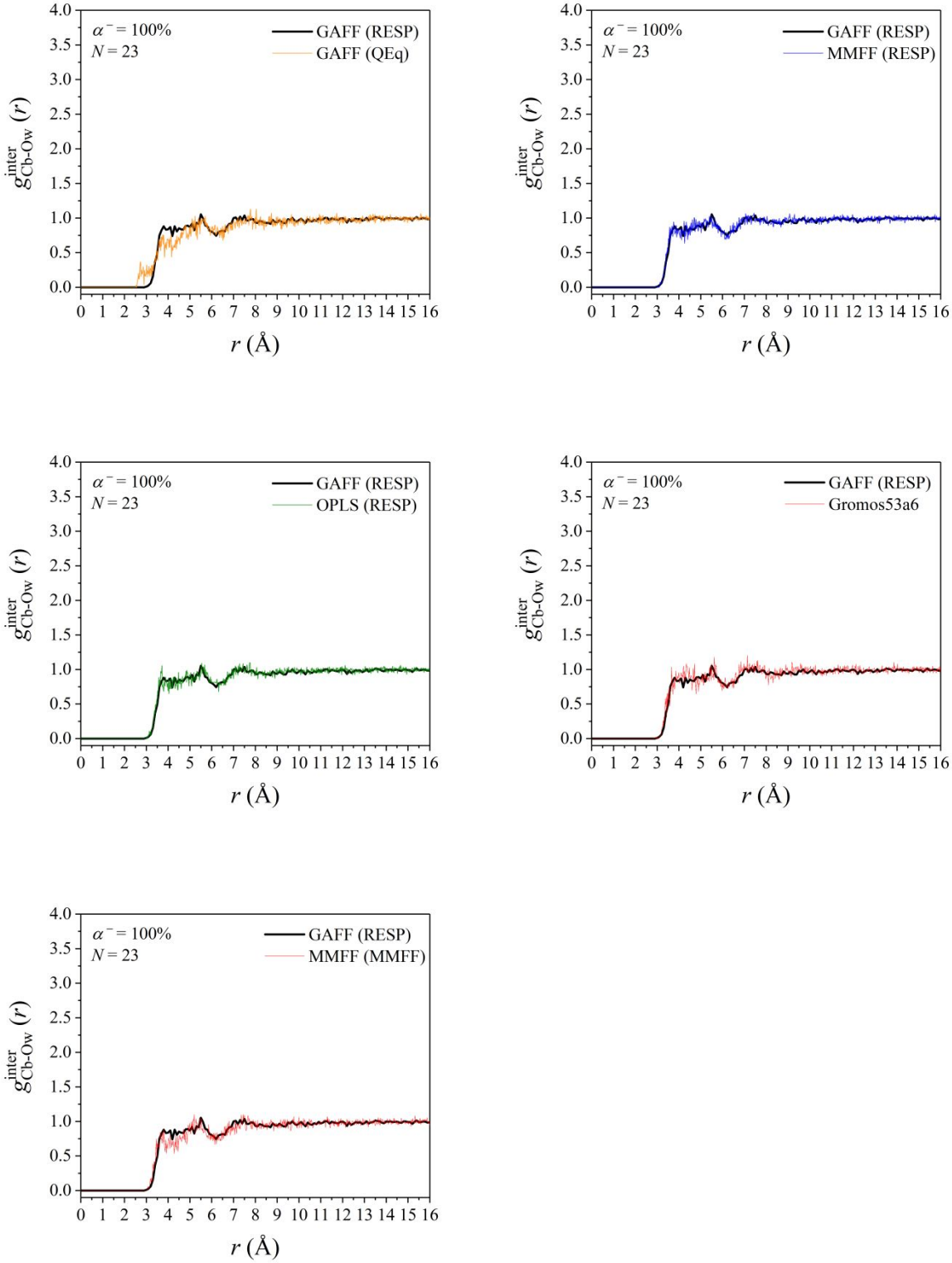

Figure S 12. Comparison of the MD predictions for $g^{\text{inter}}_{\text{Cb-Ow}}(r)$ from several molecular mechanics force fields in combination with various charge techniques and water models.

S3.2.2 Cn-Ow

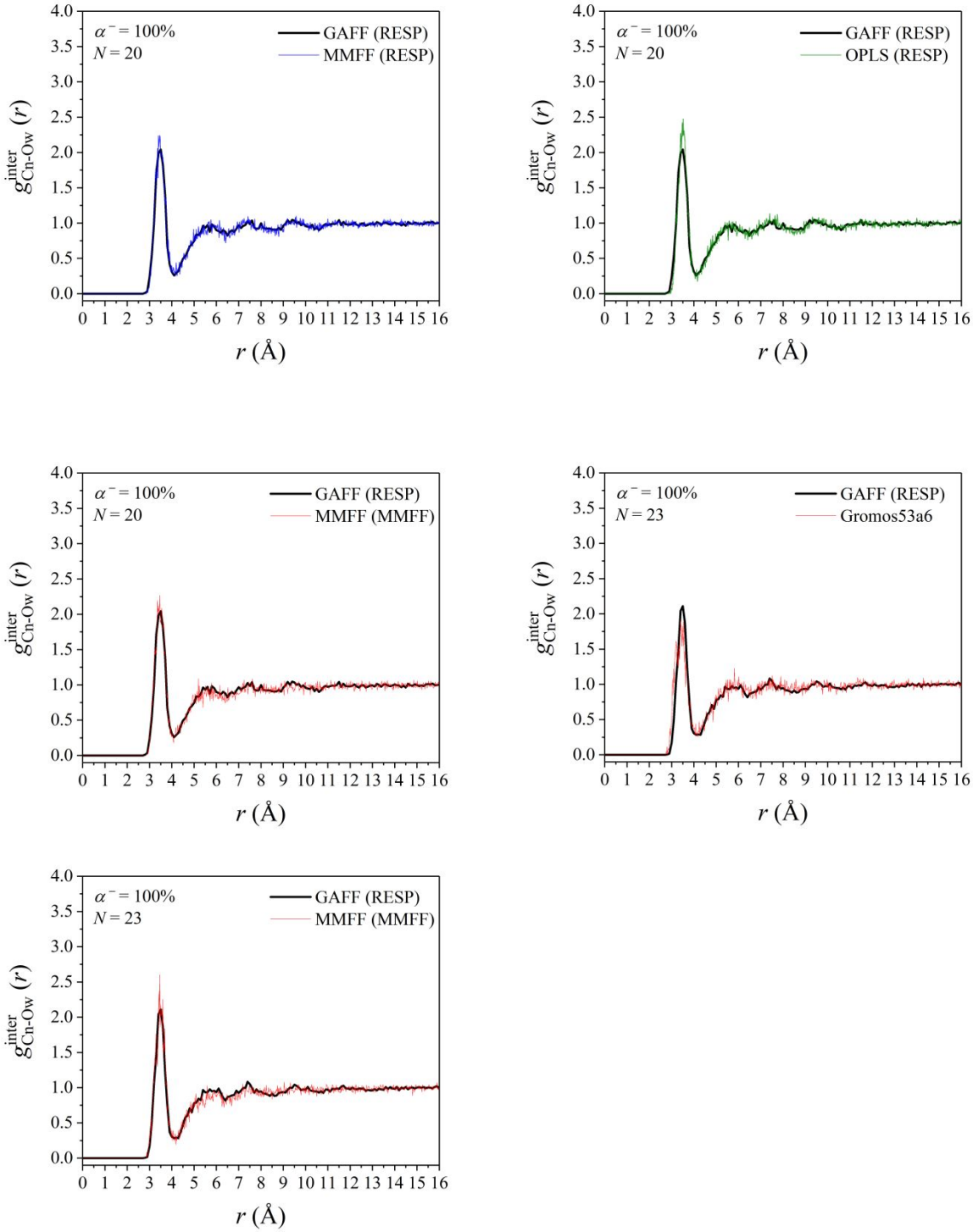

Figure S 13. Comparison of the MD predictions for $g^{\text{inter}}_{\text{Cn-Ow}}(r)$ from several molecular mechanics force fields in combination with various charge techniques and water models.

S3.2.3 Oc-Ow

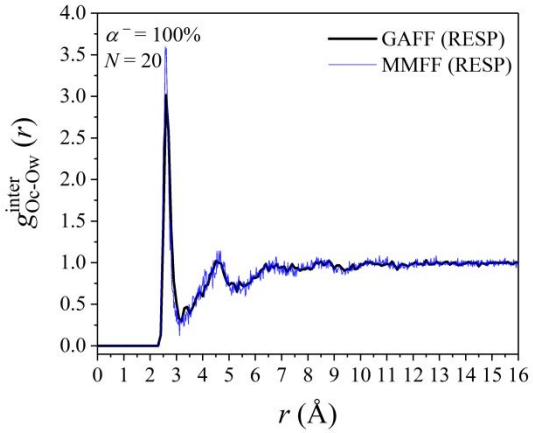
α⁻ = 100%
N = 20
GAFF (RESP)
MMFF (RESP)
g^inter_Oc-Ow (r)
r (Å)

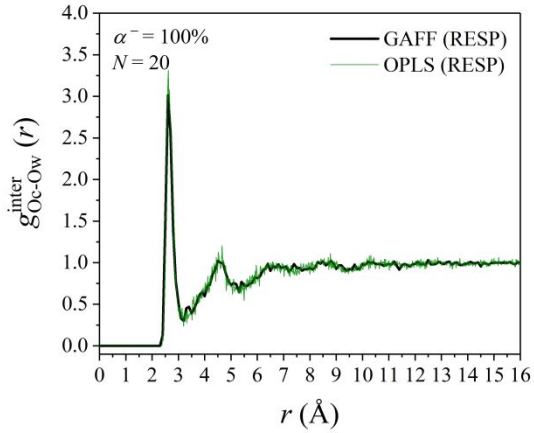
α⁻ = 100%
N = 20
GAFF (RESP)
OPLS (RESP)
g^inter_Oc-Ow (r)
r (Å)

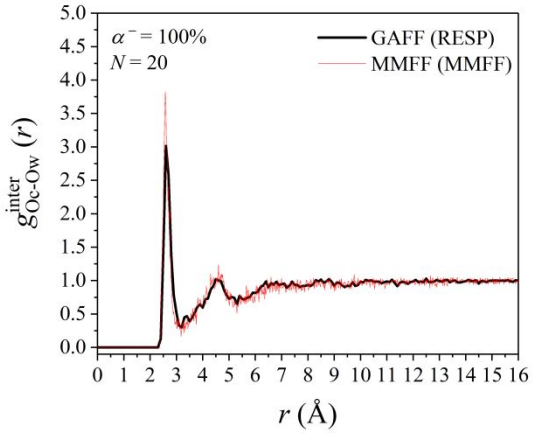
α⁻ = 100%
N = 20
GAFF (RESP)
MMFF (MMFF)
g^inter_Oc-Ow (r)
r (Å)

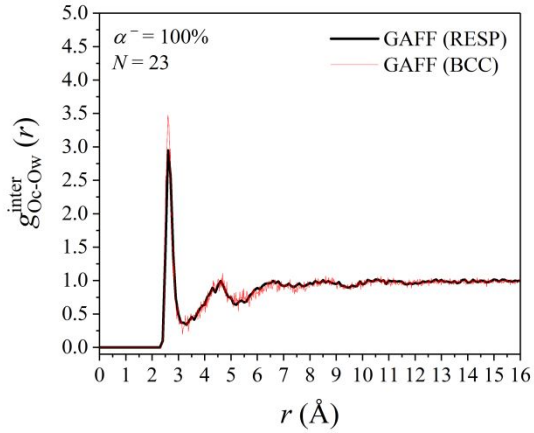
α⁻ = 100%
N = 23
GAFF (RESP)
GAFF (BCC)
g^inter_Oc-Ow (r)
r (Å)

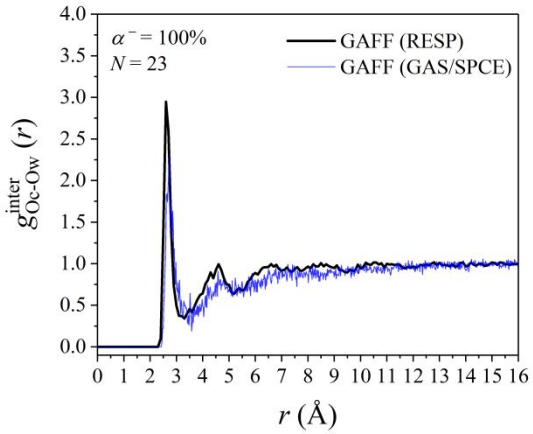
α⁻ = 100%
N = 23
GAFF (RESP)
GAFF (GAS/SPCE)
g^inter_Oc-Ow (r)
r (Å)

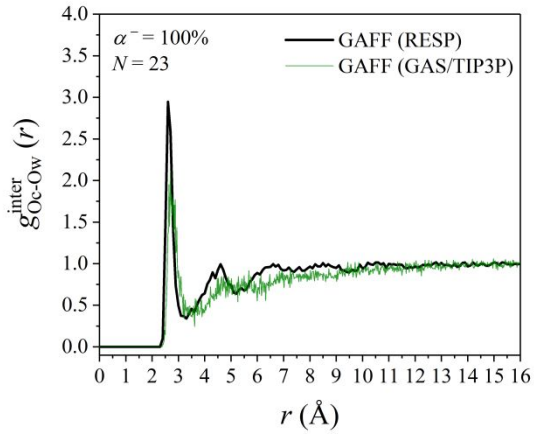
α⁻ = 100%
N = 23
GAFF (RESP)
GAFF (GAS/TIP3P)
g^inter_Oc-Ow (r)
r (Å)

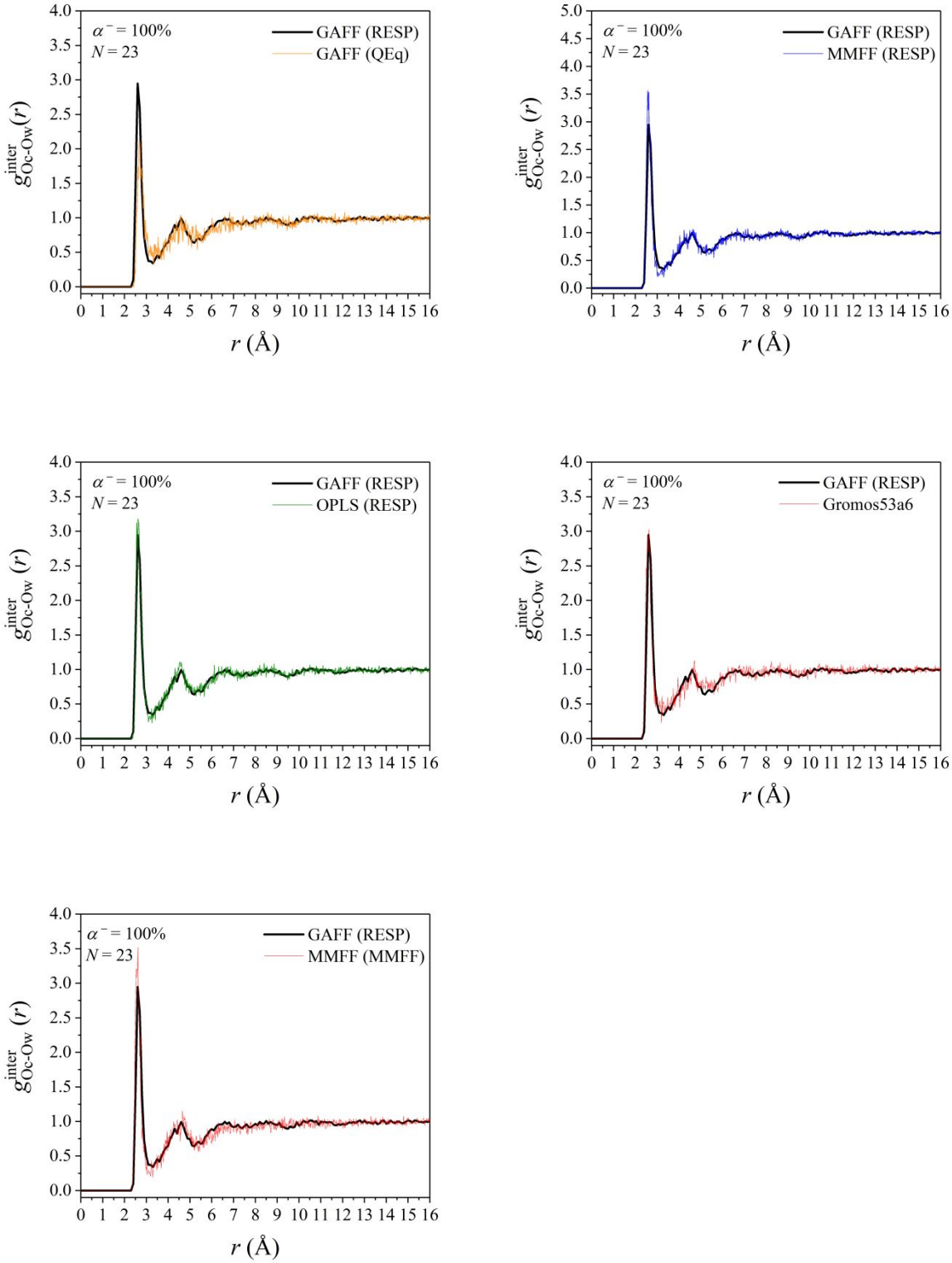

Figure S 14. Comparison of the MD predictions for $g^{\text{inter}}_{\text{Oc-Ow}}(r)$ from several molecular mechanics force fields in combination with various charge techniques and water models.

S3.3 Surface accessible area and number of H-bonds formed between the PAA chain and water molecules

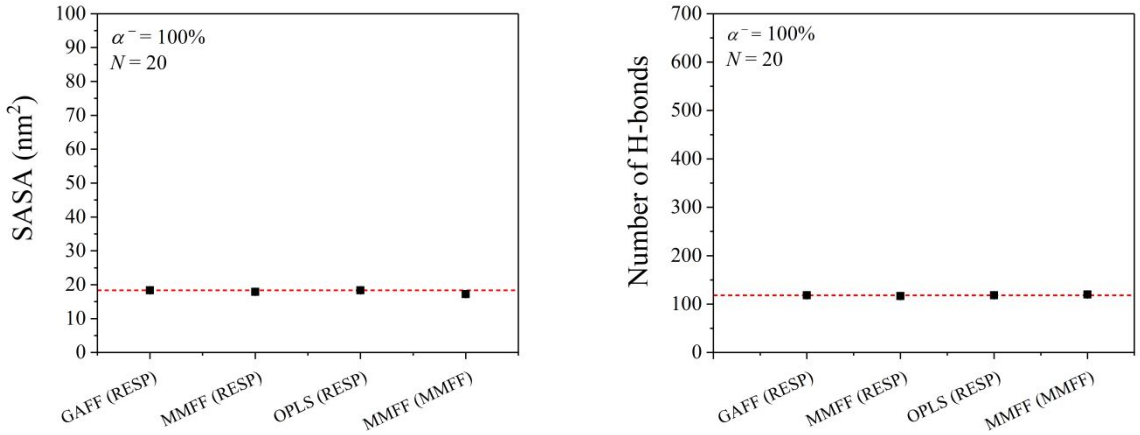

Figure S 15. Comparison of the MD predictions for the SASA and the number of H-bonds formed between PAA and water molecules from several molecular mechanics force fields in combination with various charge techniques.

S4 Average radius of gyration vs. time

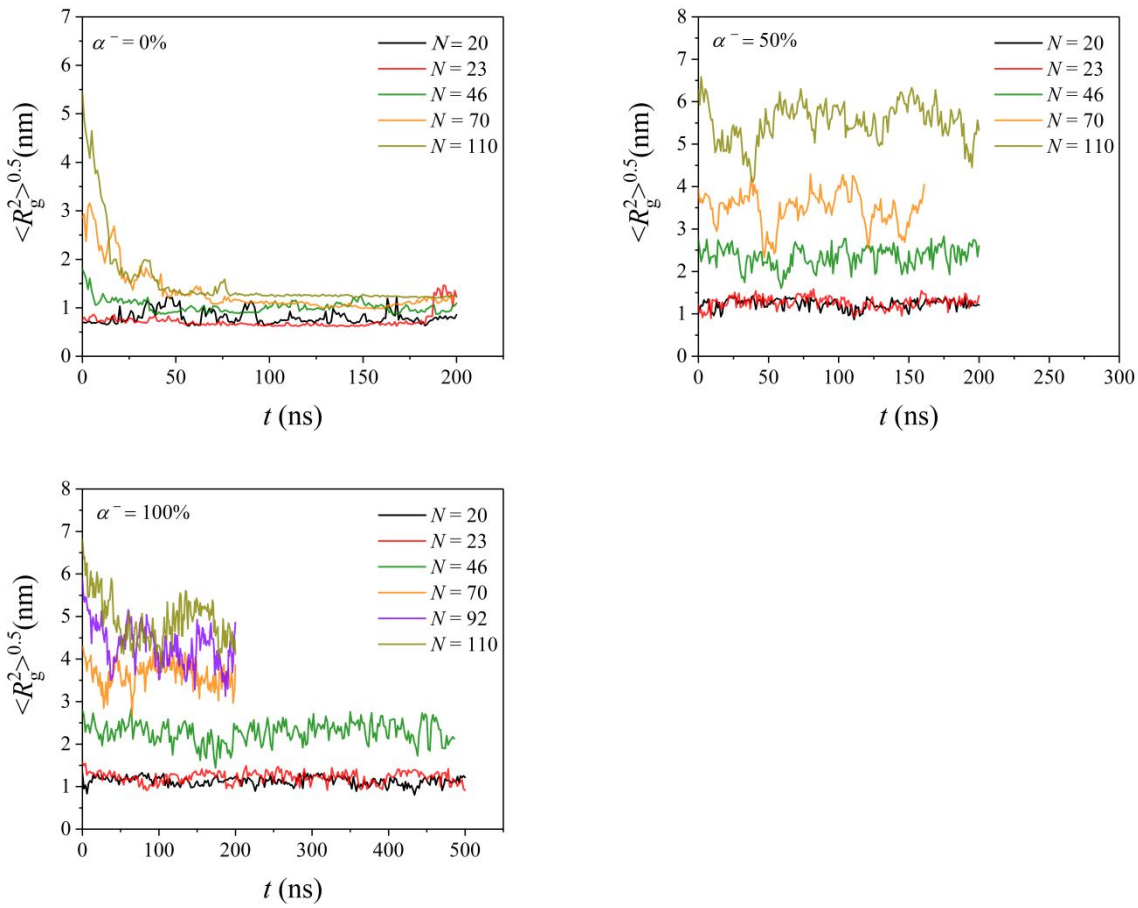

Figure S 16. Evolution of $\left\langle R_{\mathrm{g}}^{2}\right\rangle^{0.5}$ for all systems studied with time t.

S5 Average end-to-end distance vs. time

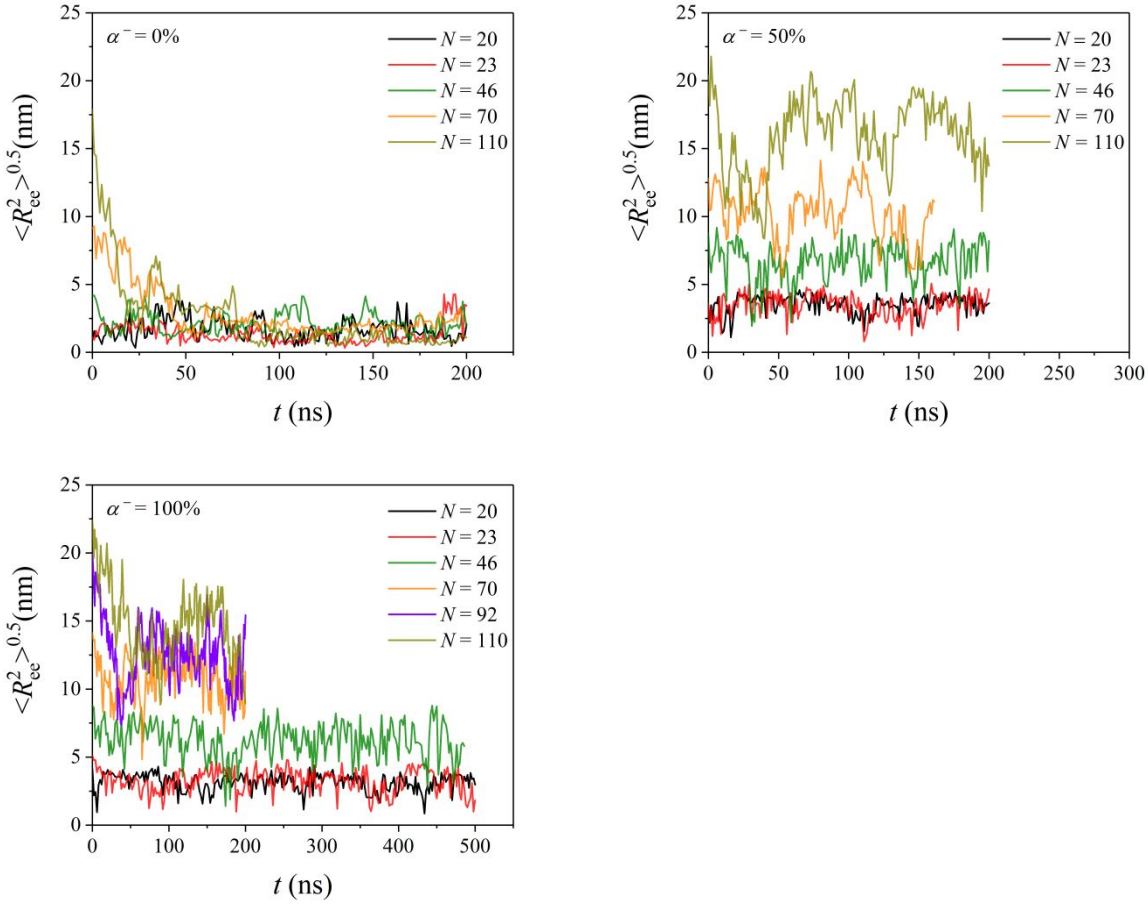

Figure S 17. Evolution of $\left\langle R_{ee}^2 \right\rangle^{0.5}$ for all systems studied with time t.

S6 Principal eigenvalues of the mean radius-of-gyration tensor

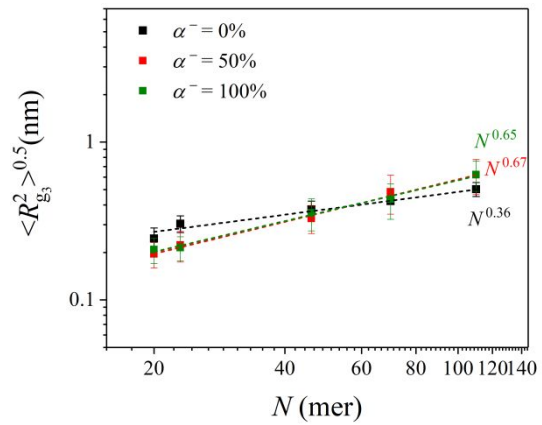

Figure S 18. The average eigenvalue $\left\langle R_{g3}^2 \right\rangle^{0.5}$ as a function of chain length N at the three different degrees of ionization.

Table S 5. Simulation predictions for the three principal eigenvalues (in nm) of the radius-of-gyration tensor at the three different degrees of ionization.

N	$\alpha^- = 0\%$			$\alpha^- = 50\%$			$\alpha^- = 100\%$		
	$\left\langle R_{g1}^2 \right\rangle^{0.5}$	$\left\langle R_{g2}^2 \right\rangle^{0.5}$	$\left\langle R_{g3}^2 \right\rangle^{0.5}$	$\left\langle R_{g1}^2 \right\rangle^{0.5}$	$\left\langle R_{g2}^2 \right\rangle^{0.5}$	$\left\langle R_{g3}^2 \right\rangle^{0.5}$	$\left\langle R_{g1}^2 \right\rangle^{0.5}$	$\left\langle R_{g2}^2 \right\rangle^{0.5}$	$\left\langle R_{g3}^2 \right\rangle^{0.5}$
20	0.62 ± 0.12	0.38 ± 0.05	0.30 ± 0.04	1.11 ± 0.15	0.40 ± 0.10	0.20 ± 0.03	1.01 ± 0.14	0.36 ± 0.07	0.21 ± 0.04
23	0.57 ± 0.27	0.36 ± 0.04	0.34 ± 0.04	1.23 ± 0.18	0.43 ± 0.11	0.21 ± 0.05	1.14 ± 0.17	0.41 ± 0.09	0.21 ± 0.04
46	0.79 ± 0.12	0.50 ± 0.06	0.37 ± 0.05	2.27 ± 0.30	0.72 ± 0.20	0.35 ± 0.06	2.21 ± 0.37	0.76 ± 0.19	0.36 ± 0.08
70	0.86 ± 0.08	0.53 ± 0.02	0.42 ± 0.02	3.27 ± 0.51	0.95 ± 0.24	0.48 ± 0.13	3.29 ± 0.35	0.90 ± 0.24	0.43 ± 0.11
110	0.95 ± 0.04	0.62 ± 0.03	0.49 ± 0.05	5.39 ± 0.45	1.43 ± 0.37	0.64 ± 0.15	5.12 ± 0.48	1.40 ± 0.32	0.62 ± 0.13

S7 Persistence length

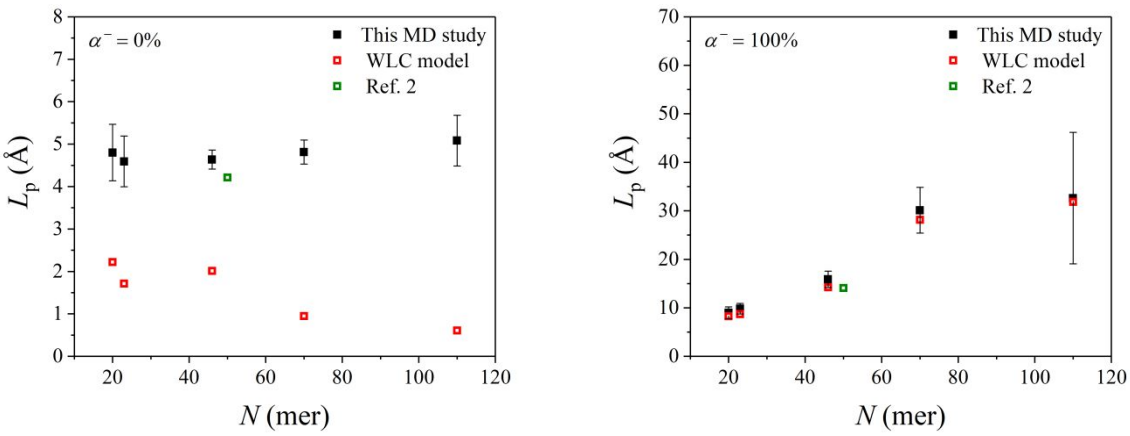

Figure S 19. Comparison of the L_p values obtained from the WLC model, the present MD study and previous study[2] as a function of chain length *N*.

S8 Radial distribution functions

S8.1 Effect of several pairs towards solvation of the PAA chain

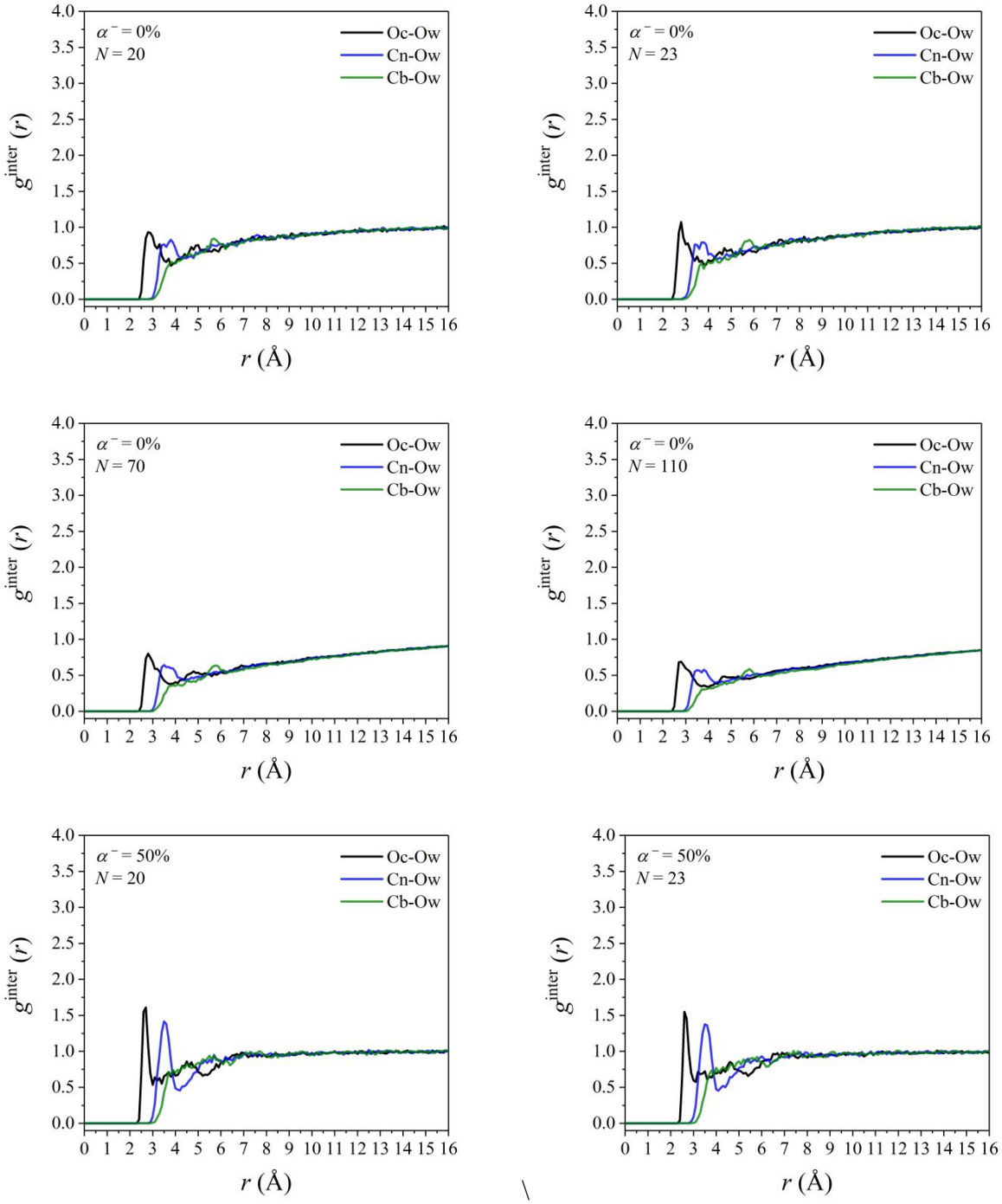

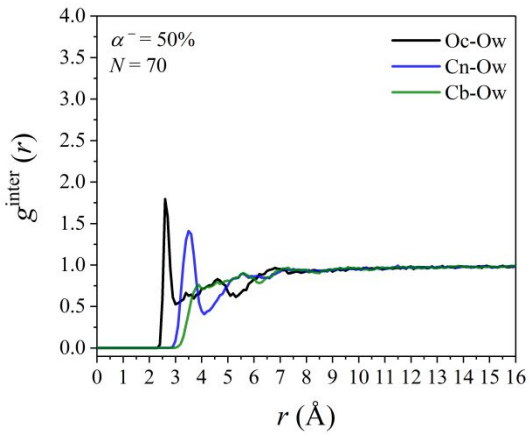
α⁻ = 50%
N = 70
Oc-Ow
Cn-Ow
Cb-Ow
g^inter (r)
r (Å)

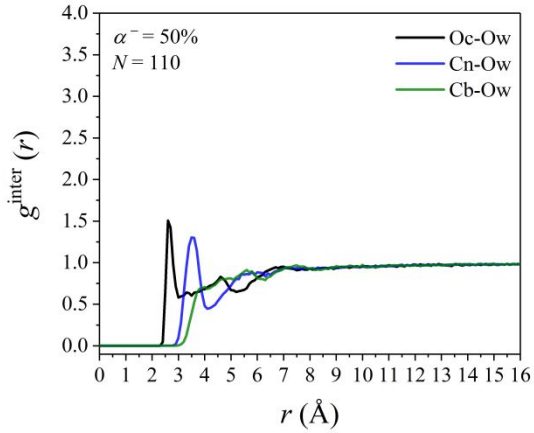
α⁻ = 50%
N = 110
Oc-Ow
Cn-Ow
Cb-Ow
g^inter (r)
r (Å)

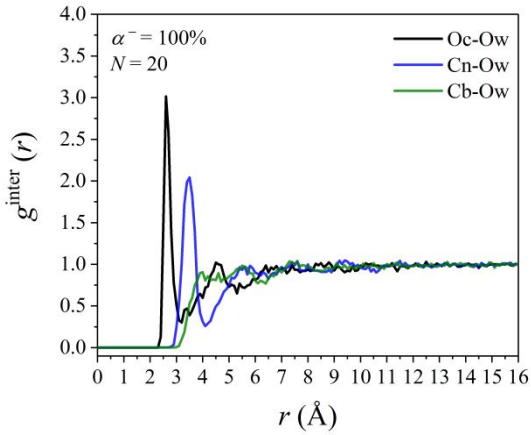
α⁻ = 100%
N = 20
Oc-Ow
Cn-Ow
Cb-Ow
g^inter (r)
r (Å)

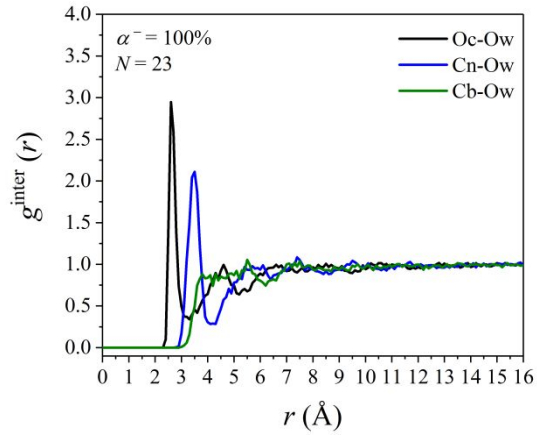
α⁻ = 100%
N = 23
Oc-Ow
Cn-Ow
Cb-Ow
g^inter (r)
r (Å)

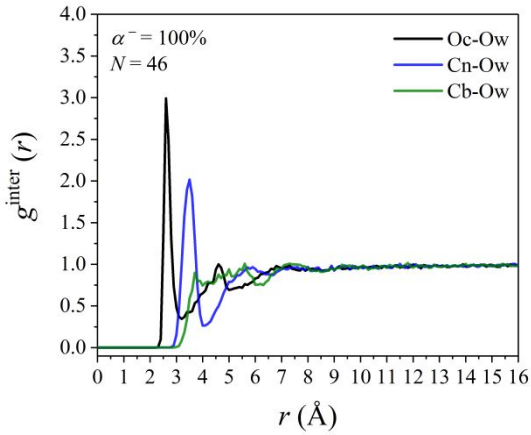
α⁻ = 100%
N = 46
Oc-Ow
Cn-Ow
Cb-Ow
g^inter (r)
r (Å)

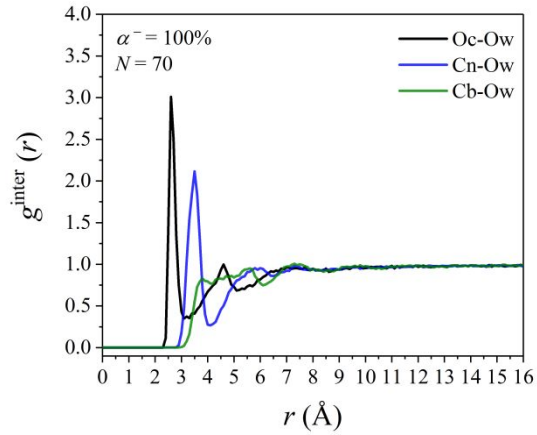
α⁻ = 100%
N = 70
Oc-Ow
Cn-Ow
Cb-Ow
g^inter (r)
r (Å)

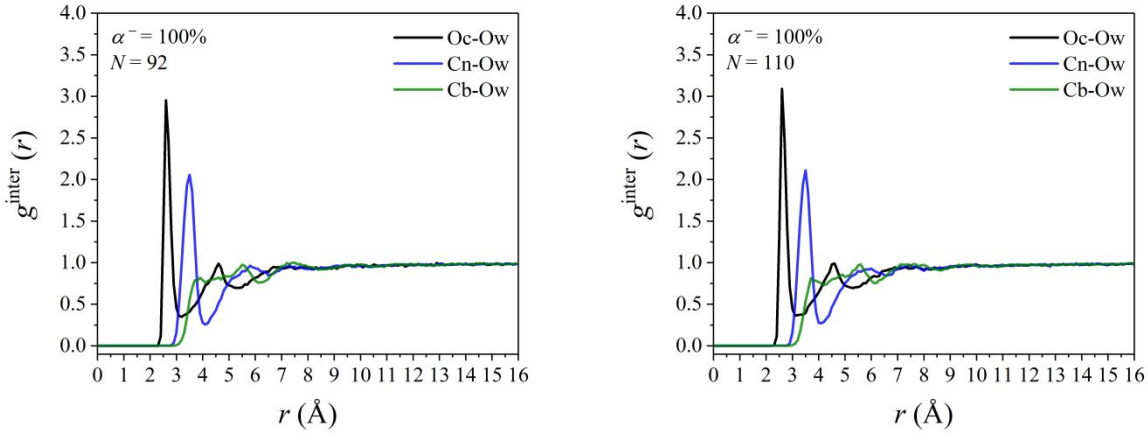

Figure S 20. Cb-Ow, Cn-Ow and Oc-Ow radial intermolecular distribution functions for various chain lengths *N* and degrees of ionization α^-.

S8.2 Effect of degree of ionization

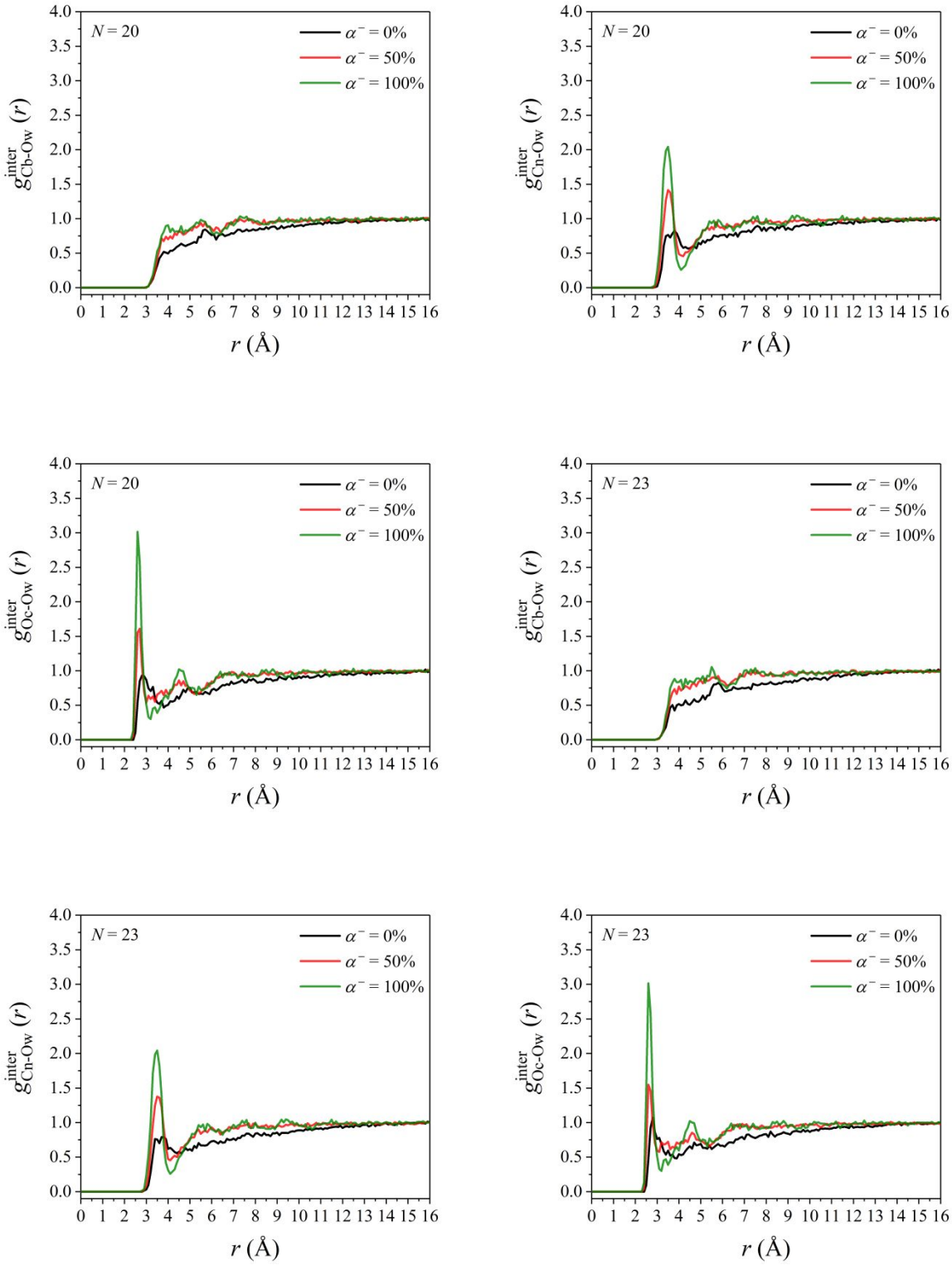

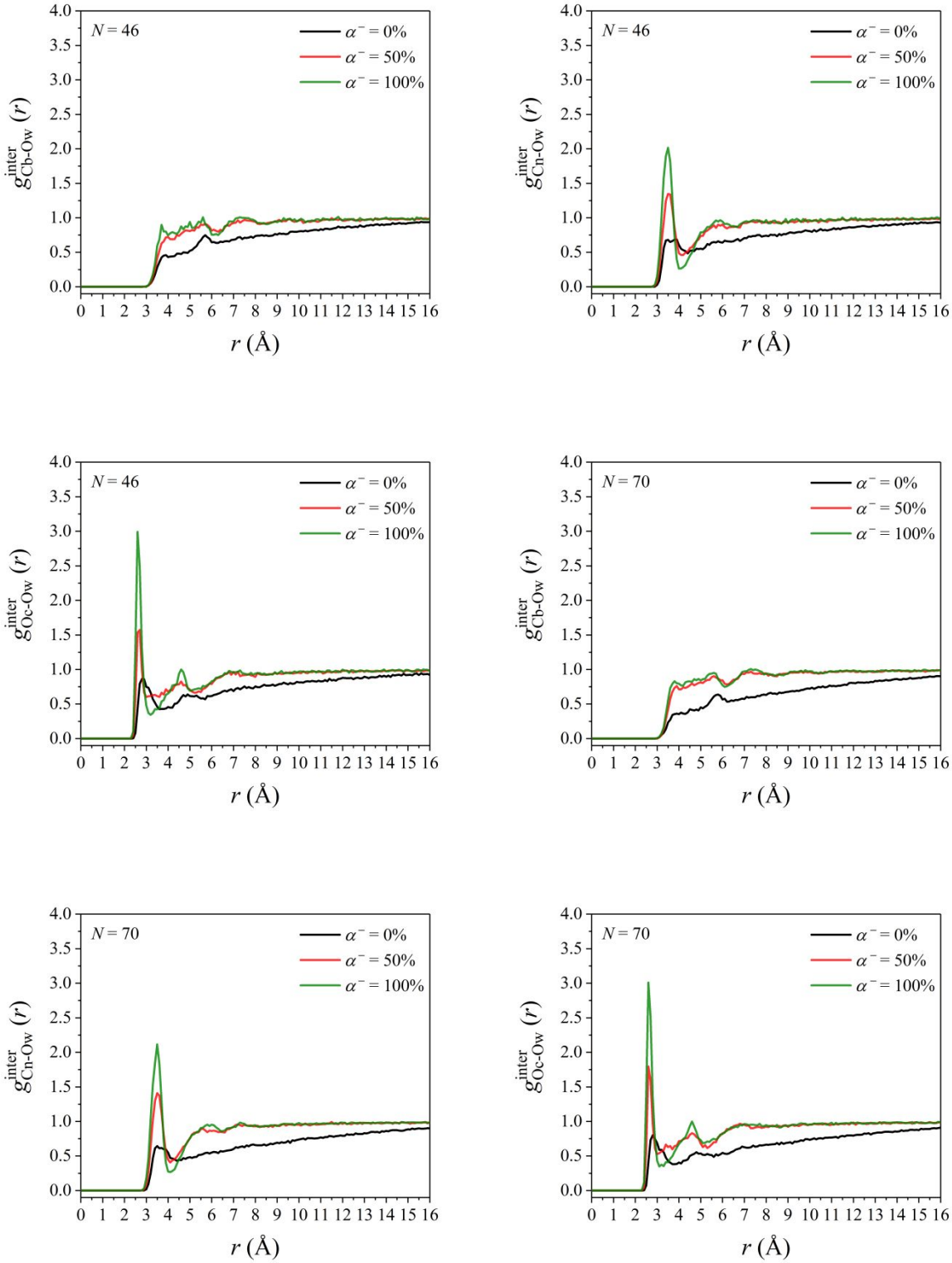
N = 46
α⁻ = 0%
α⁻ = 50%
α⁻ = 100%
g^inter_Cb-Ow (r)
g^inter_Cn-Ow (r)
g^inter_Oc-Ow (r)
N = 70
r (Å)

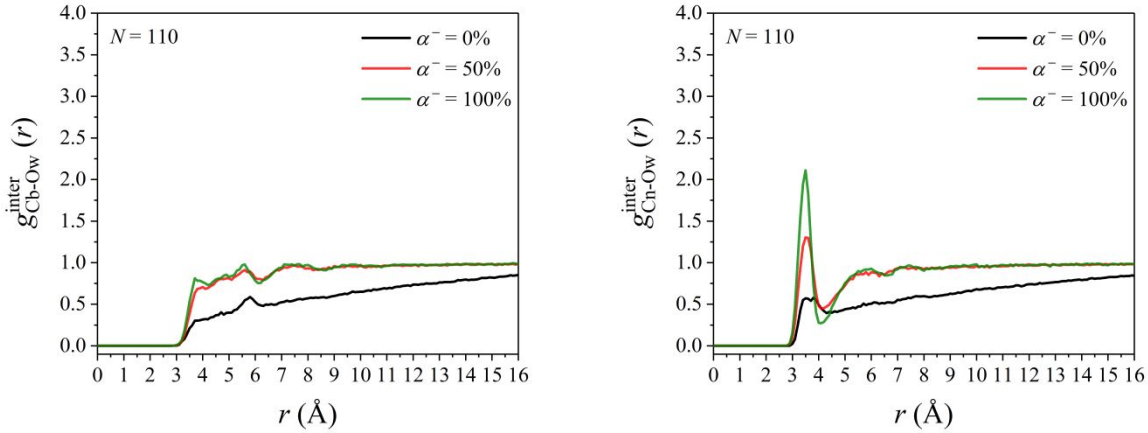

Figure S 21. Cb-Ow, Cn-Ow and Oc-Ow radial intermolecular distribution functions for various chain lengths *N* and degrees of ionization α^-.

S8.3 Cb-Ow

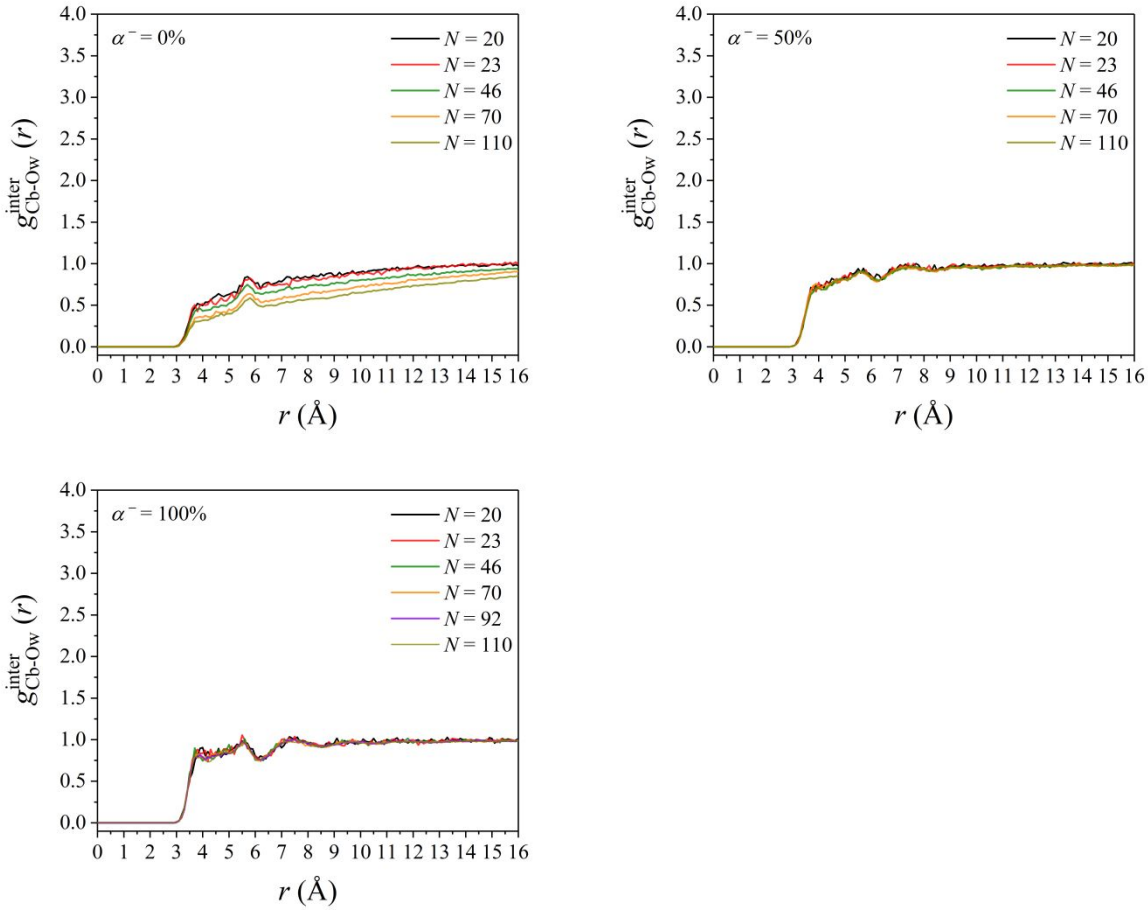

Figure S 22. Cb-Ow radial intermolecular distribution function for various chain lengths N and degrees of ionization α^-.

S8.4 Cn-Ow

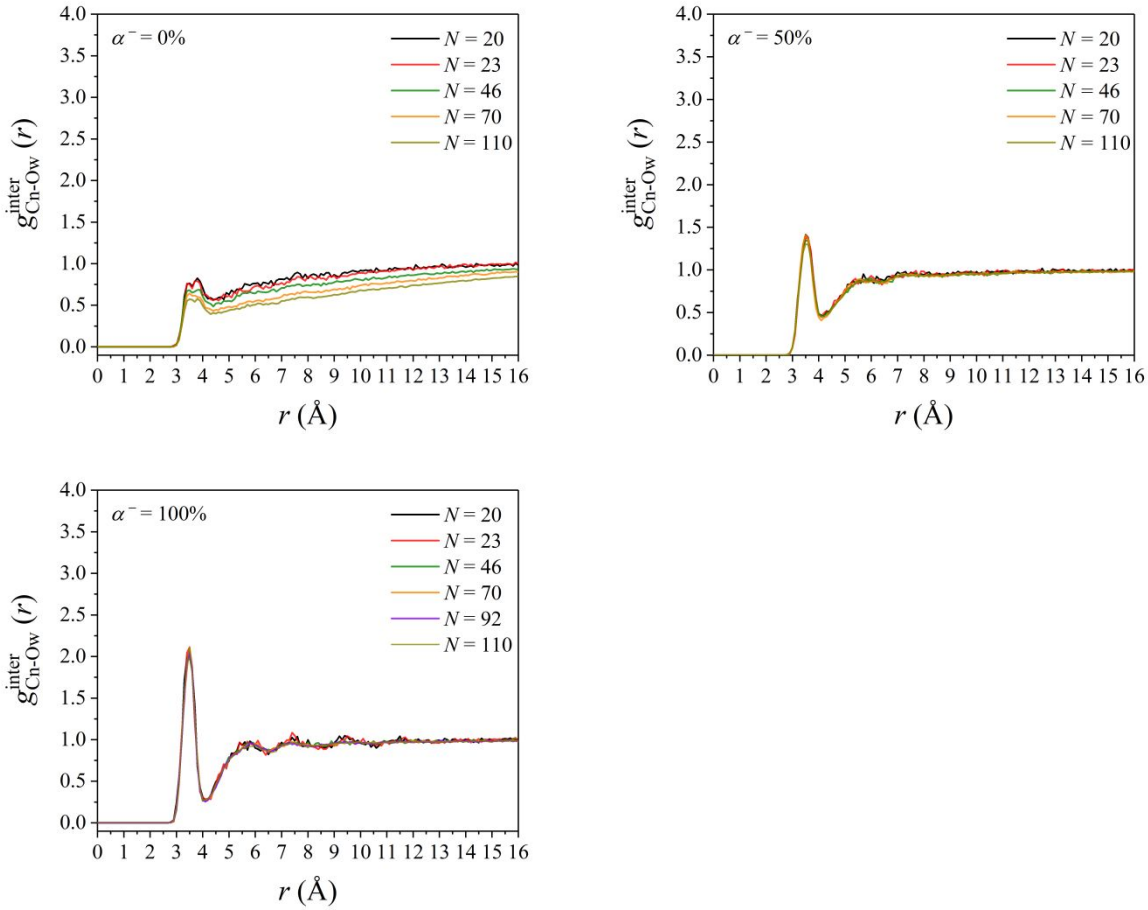

Figure S 23. Cn-Ow radial intermolecular distribution function for various chain lengths N and degrees of ionization α^-.

S9 Surface accessible area and number of H-bonds formed between the PAA chain and water molecules

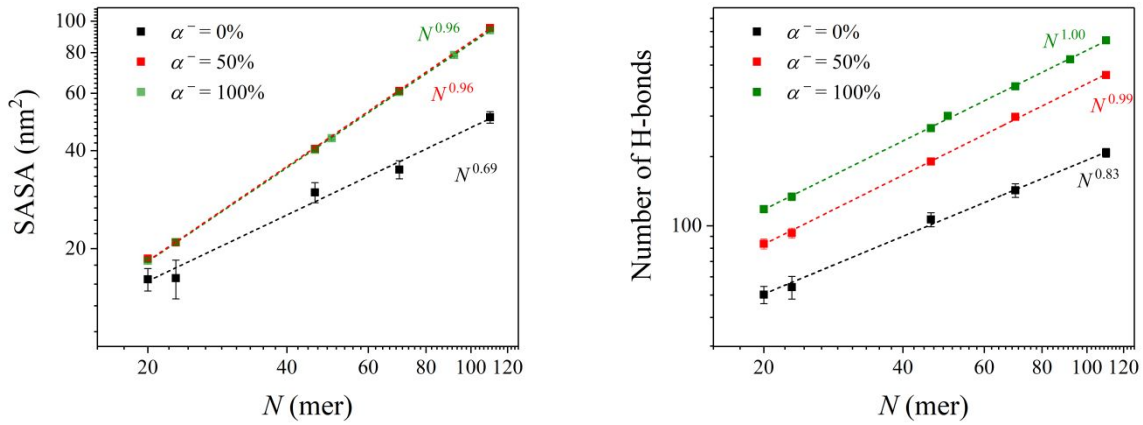

Figure S 24. Scaling of SASA and number of H-bonds with chain length N for the three different degrees of ionization α^-.

S10 Log(msd) vs. log(t)

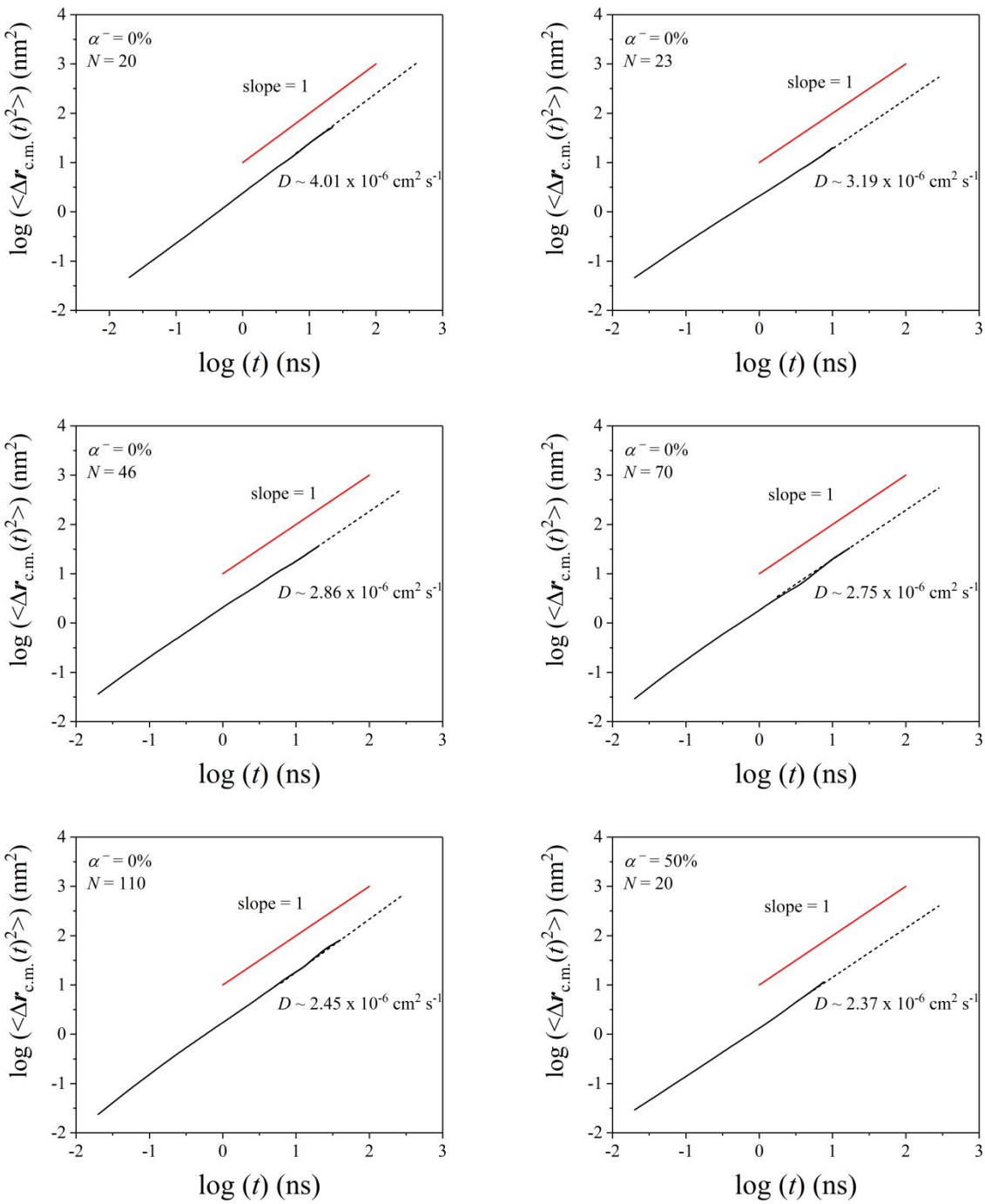

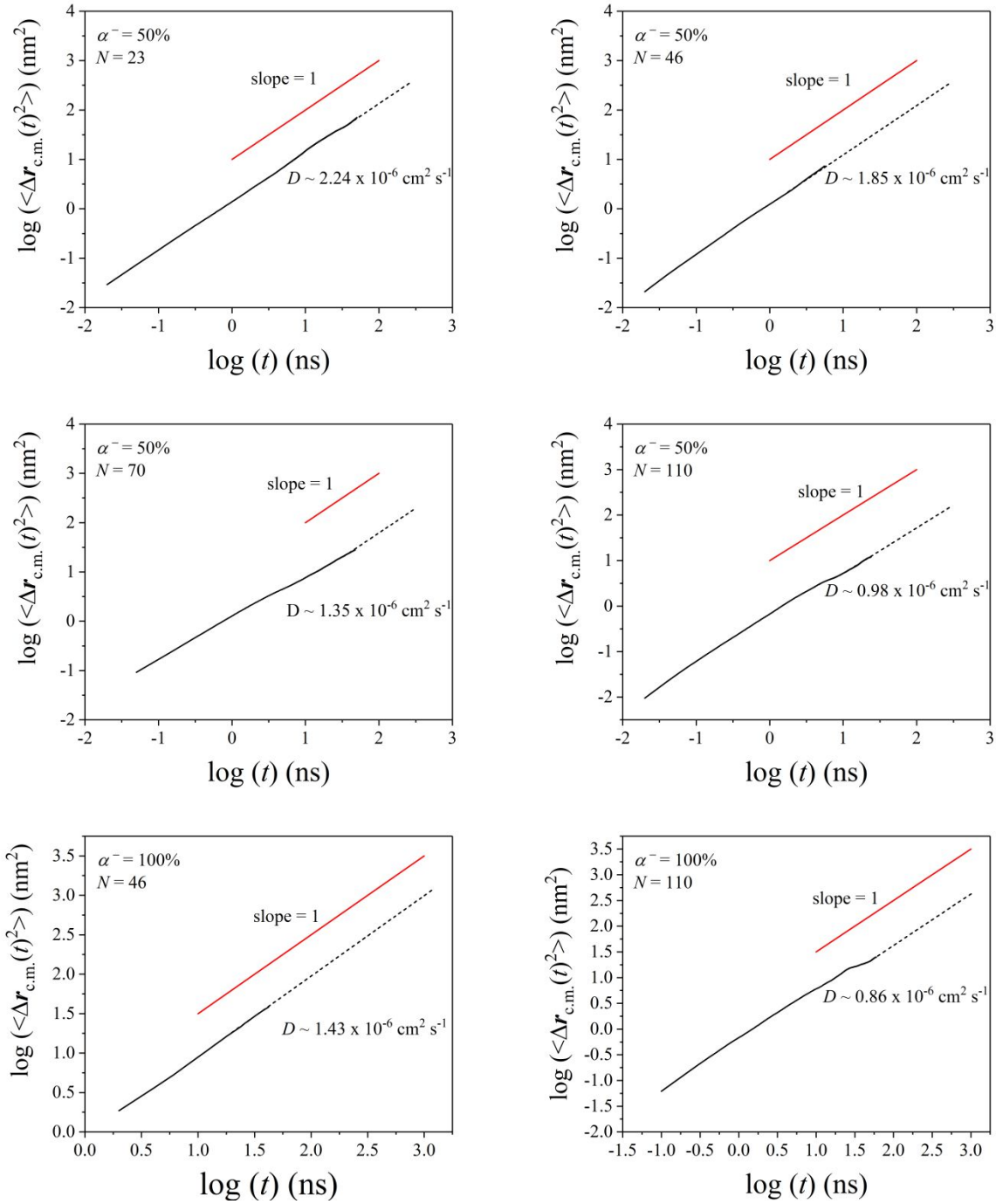

Figure S 25. Log-log plot of the mean-square displacement (MSD) of the PAA chain center-of-mass versus time *t* for various chain lengths *N* and degrees of ionization α^-.

S11 Conformational transitions of the PAA chain (visualization)

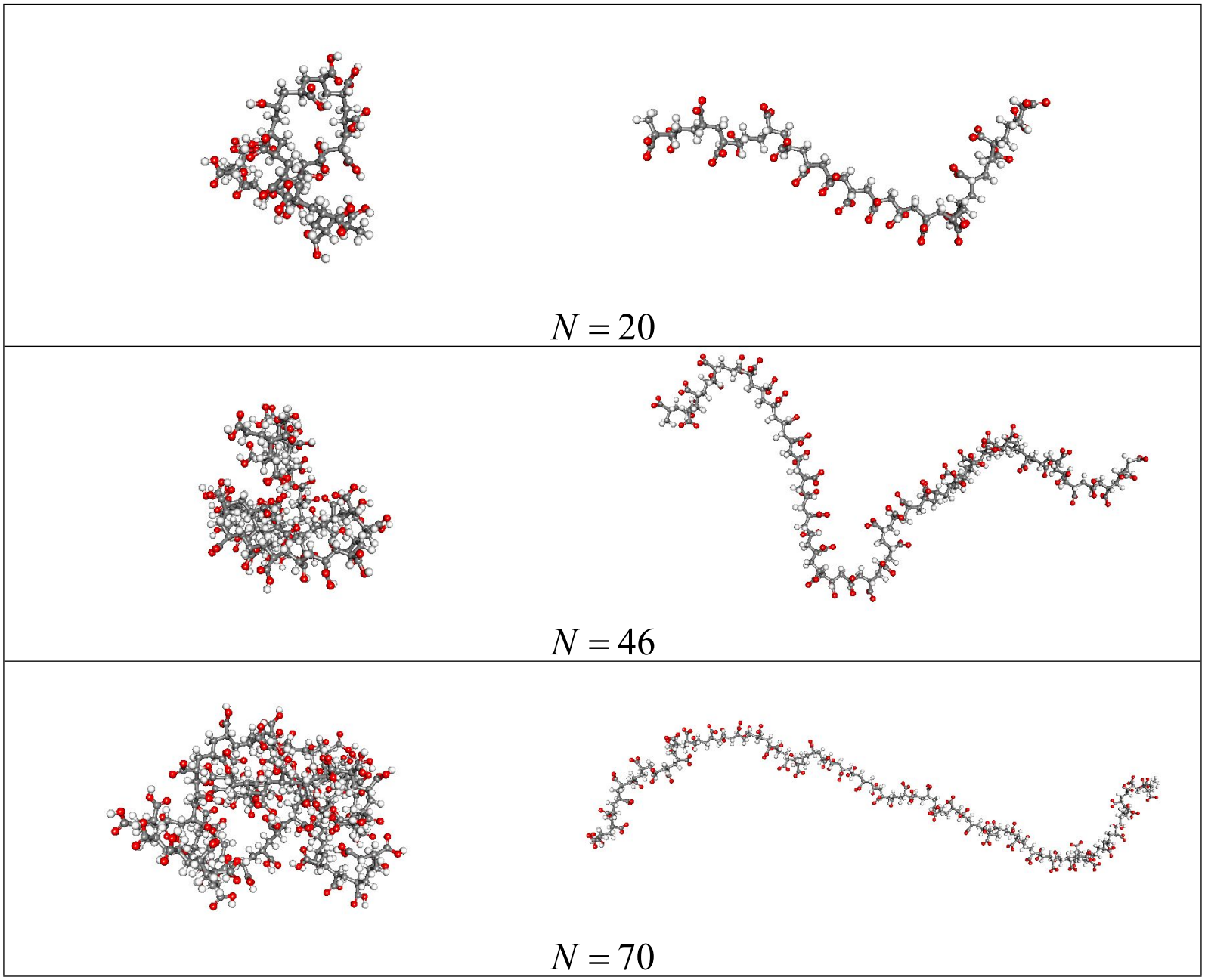

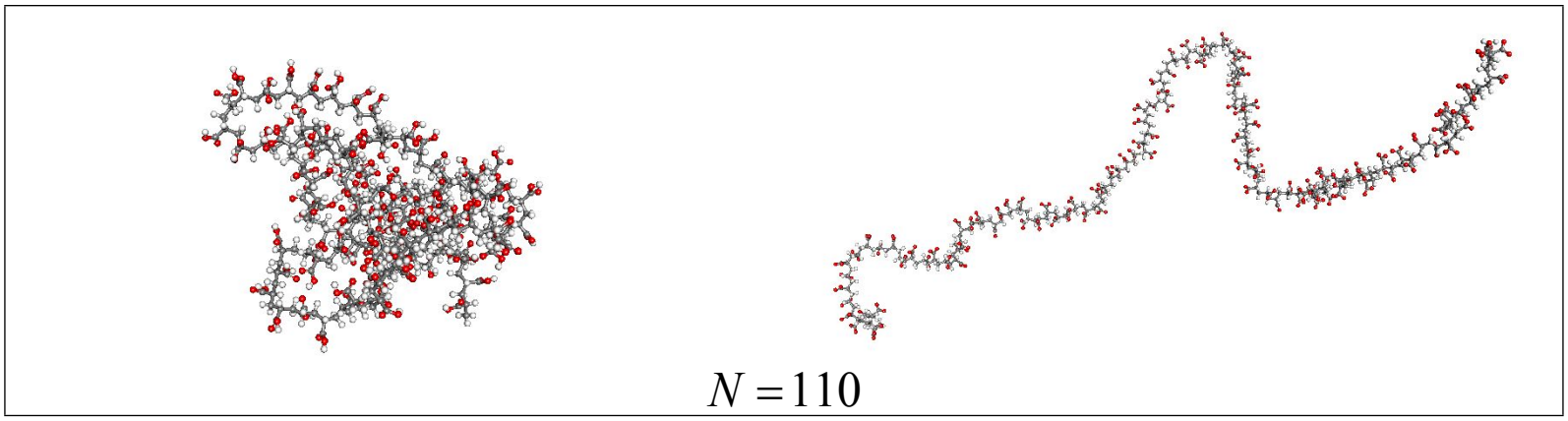

Figure S 26. Characteristic MD snapshots highlighting the conformational transitions that a PAA chain undergoes at 0% (left-hand side) and 100% (right-hand side) degree of ionization (after approximately 150 ns of simulation time) for various chain lengths *N*.

References

1. Sulatha, M.S.; Natarajan, U. Origin of the difference in structural behavior of poly (acrylic acid) and poly (methacrylic acid) in aqueous solution discerned by explicit-solvent explicit-ion MD simulations. *Ind. Eng. Chem. Res.* **2011,** *50*, 11785-11796.
2. Cranford, S.W.; Buehler, M.J. Variation of weak polyelectrolyte persistence length through an electrostatic contour length. *Macromolecules* **2012,** *45*, 8067-8082.